This paper is published as part of a *PCCP* themed issue on dynamic nuclear polarization

Guest Editors: Robert Griffin and Thomas Prisner

Editorials

Communications

Papers

Optimization of dynamic nuclear polarization experiments in aqueous solution at 15 MHz/9.7 GHz: a comparative study with DNP at 140 MHz/94 GHz

Maria-Teresa Türke,[a] Igor Tkach,[a] Marcel Reese,[a] Peter Höfer[b] and Marina Bennati*[a]

Received 9th February 2010, Accepted 23rd April 2010
First published as an Advance Article on the web 8th May 2010
DOI: 10.1039/c002814m

Dynamic nuclear polarization is emerging as a potential tool to increase the sensitivity of NMR aiming at the detection of macromolecules in liquid solution. One possibility for such an experimental design is to perform the polarization step between electrons and nuclei at low magnetic fields and then transfer the sample to a higher field for NMR detection. In this case, an independent optimization of the polarizer and detection set ups is required. In the present paper we describe the optimization of a polarizer set up at 15 MHz ^{1}H NMR/9.7 GHz EPR frequencies based on commercial hardware. The sample consists of the nitroxide radical TEMPONE-D,^{15}N in water, for which the dimensions were systematically decreased to fit the homogeneous B_1 region of a dielectric ENDOR resonator. With an available B_1 microwave field up to 13 G we observe a maximum DNP enhancement of −170 at room temperature by irradiating on either one of the EPR lines. The DNP enhancement was saturated at all polarizer concentrations. Pulsed ELDOR experiments revealed that the saturation level of the two hyperfine lines is such that the DNP enhancements are well consistent with the coupling factors derived from NMRD data. By raising the polarizing field and frequencies 10-fold, *i.e.* to 140 MHz ^{1}H/94 GHz EPR, we reach an enhancement of −43 at microwave field strengths ($B_1 \approx 5$ G). The results are discussed in view of an application for a DNP spectrometer.

Introduction

Dynamic nuclear polarization (DNP) of nuclei in liquid solutions containing paramagnetic centres has been studied since the early years of magnetic resonance to obtain information about molecular motion and electron-nuclear spin relaxation.[1,2] In the past few years, this technique has attracted a lot of attention again since it could provide a means to overcome the sensitivity limits in solution and solid state NMR towards studying macromolecular complexes.[3–5] A few approaches have been proposed to combine DNP with solution NMR at high fields (see also other contributions in this issue). In a first approach, the sample is polarized in the solid state at very low temperature and is subsequently dissolved very rapidly for NMR detection at room temperature.[5,6] To avoid sample freezing two other methods have lately been examined: (a) *in situ* polarization and NMR detection at high fields, *i.e.* 9 T/260 GHz EPR[7,8] and finally (b) polarization at low fields (0.35 T, 9.7 GHz EPR) and detection at very high fields 14 T/600 MHz ^{1}H NMR after sample shuttling.[9,10] Within these activities, several groups reported substantial enhancements of water resonances in the solution state at different fields (up to 14 T) using TEMPO or nitroxide derivatives.[2,7,10–15,19] The studies lead to re-examination of the Overhauser mechanism and its frequency dependence, as proposed in the early 60th and 70th; however the key issue about the maximal achievable enhancement at a certain frequency, important for the design and optimization of DNP spectrometers, is still under debate.

According to Overhauser,[16,17] the DNP enhancement ε in liquids depends on four factors:

$$\varepsilon = \frac{\langle I_z \rangle}{I_0} = 1 - \xi f s \frac{|\gamma_s|}{\gamma_I} \qquad (1)$$

i.e. the gyromagnetic ratios of the electron and the observed nucleus γ_S/γ_I, the saturation factor of the EPR line s, the leakage factor f and the coupling factor ξ (sometimes also denoted as ρ). In principle, the maximal achievable enhancement should be predictable from eqn (1) if the saturation and the leakage factor could be made experimentally close to one while the coupling factor is determined independently from NMRD (nuclear magnetic resonance dispersion) measurements. We have recently employed NMRD to determine the coupling and leakage factor of TEMPOL in water[13,14,18] at 0.35 T/15 MHz ^{1}H NMR and estimated that the maximal enhancement of the water protons at room temperature should be about −225. From comparison with our first experimental data of −100[13] and −140[14] for ^{14}N and ^{15}N labelled TEMPONE, respectively, we concluded that the enhancements were likely power limited. Subsequent studies by Armstrong *et al.*,[19–21] who developed a model to extrapolate the coupling factor from DNP data, pointed out that the maximal enhancement and the derived coupling factor at

[a] *Max Planck Institute for Biophysical Chemistry, Am Faßberg 11, 37077 Göttingen, Germany. E-mail: bennati@mpibpc.mpg.de*
[b] *Bruker Biospin, EPR Division, Rheinstetten, Germany*

0.35 T might be substantially lower than those predicted by our studies, *i.e.* $\xi \approx 0.22$ *versus* 0.36 from NMRD. The authors argued that our observation of high DNP enhancements could arise from heating effects rather than from the large coupling factor, however a failure of the NMRD approach seemed without fundamental justification. Most recent molecular dynamic simulations by Sezer *et al.*,[22] used to calculate the correlation functions for electron nuclear interactions, suggested that the coupling factor at 0.35 T/9.7 GHz/15 MHz could be around 0.3, *i.e.* slightly lower than the NMRD value but substantially higher than the value predicted by ref. 21.

The discussion prompted us to carry out a systematic study of the experimental parameters that should affect the evaluation of the DNP enhancement, in particular the dependence on sample heating, cavity and magnetic field instabilities and inhomogeneities, effective microwave field strength and distribution through the sample, and sample dimensions. Two hardware components have been examined: (a) the microwave excitation system comprehending resonator, sample and amplifier, and (b) the NMR signal detection system. The microwave resonator determines the effective magnetic and electric field distribution at the sample in combination with the available microwave power. Although in the literature DNP enhancements are routinely reported as a function of power, the saturation factor and thus the enhancement, are rather determined by the effective microwave field strength B_1 over the entire sample. The difference in the effective B_1 fields at the sample position for set ups with comparable microwave power might have led to a variety of enhancements observed in the past. The B_1 field can be measured by EPR transient nutation experiments as a function of the sample size and position. Furthermore, the position of the absorption dip can easily be shifted by heating effects and needs monitoring during the DNP experiment.

The electric field at the sample causes power losses and heating, which might damage the sample but also prevents a proper evaluation of the Overhauser coupling factor. Since a measurement of the electric field distribution over the sample is not straightforward, we propose to estimate the temperature raise from the dielectric losses causing the change in the quality factor of the cavity. For a large sample size (*i.e.* 0.9 mm inner diameter) the temperature in the sample can be concomitantly monitored by a suitable sensor. Finally, the NMR signal detection usually consists of a low frequency NMR spectrometer operating within an EPR electromagnet, not always equipped with a field lock system. Magnetic field shifts on the order of Gauss can cause distortion of the FID during the accumulation time of the NMR signal. The same field shift can also cause an off-resonant drift of the EPR signal with a substantial effect on the DNP enhancement due to the very narrow lines of nitroxide radicals (about 0.5–2 G in the concentration range used here).

Overall, the study presented here led to an observation of an enhancement of -170 by continuous wave irradiation on either EPR line of TEMPONE-D,^{15}N. The enhancement displays saturation, *i.e.* it cannot be increased by increasing the microwave magnetic field between about 4 and 13 G. Therefore, we believe that we have reached the limit of achievable saturation and enhancement with continuous irradiation. We also describe a comparative study at the 10-fold field and frequency.

Experimental

The DNP spectrometer operating at 0.35 T (9.7 GHz EPR, 15 MHz ^{1}H NMR) is based on a commercial Bruker EMX X-band EPR spectrometer and a Bruker Minispec (2–65 MHz) for microwave irradiation and NMR detection, respectively (see Fig. 1). The set up is also compatible with a pulsed microwave bridge (Bruker ElexSys 580) if pulsed microwave radiation is required. The microwave output of the bridge is amplified by a solid state 4 W microwave amplifier (Bruker AmpX10). For higher power excitations a 34 W TWT amplifier (Varian) was employed. Subsequently, the microwave is fed into an ENDOR (electron nuclear double resonance) probe head consisting of a dielectric resonator (Bruker EN4118X-MD4) and RF coils matched additionally to a tuneable RF circuit[13] for NMR detection. The resonator displays a region of about $4 \times 4 \times 4$ mm around its center, in which the microwave B_1 magnetic field is homogeneous. Outside this region, B_1 falls rapidly (within mm) to zero. Conversely, the electric field distribution is not easily specified and was tested in these experiments with different sample sizes by measuring the dielectric losses.

All DNP experiments were performed under critical coupling of the microwave cavity to obtain the maximal B_1 field. This setting required an additional option for continuously monitoring the cavity dip during cw irradiation. Two circulators were introduced, one between the microwave bridge and the amplifier, and one between the latter and the cavity (Fig. 1). The high reflected power from the probe is deviated by circulator (2) into a side arm, attenuated by 40 dB and fed *via* circulator (1) into the bridge for detection. In this manner we were able to observe a substantial frequency shift of the cavity dip while irradiating at high powers (34 W), caused by severe heating of the cavity's inner surfaces. In order to stabilize the temperature inside the cavity, cold N_2 gas was constantly flushed into the cavity. By applying a nitrogen flow of 10 l min^{-1} it was feasible to avert the shift completely and stabilize the dip at one position during the experiment. The N_2 gas flow was used in all DNP experiments (if not stated otherwise). Samples were typically irradiated for 0.5–4 s while monitoring the microwave power with a power meter (Agilent N1911A or Gigatronics 80350A). The irradiation time t_{mw} required to reach the optimal enhancement depends on the radical concentration and was experimentally determined for each sample.

The static magnetic field B_0 produced by an electromagnet was set at the position of one of the EPR lines to fulfil the EPR resonance condition. The DNP spectrometer is equipped with a field frequency lock (FF-lock), which in combination with the NMR-Gaussmeter permits precise settings of the magnetic field position. For NMR detection a $\pi/2$ RF pulse was applied after microwave irradiation and a subsequent NMR free induction decay was recorded using an 8 step phase cycle. All events in the DNP experiments were synchronised by the NMR spectrometer, which gated the microwave amplifier before signal acquisition. To ensure linear behaviour of the

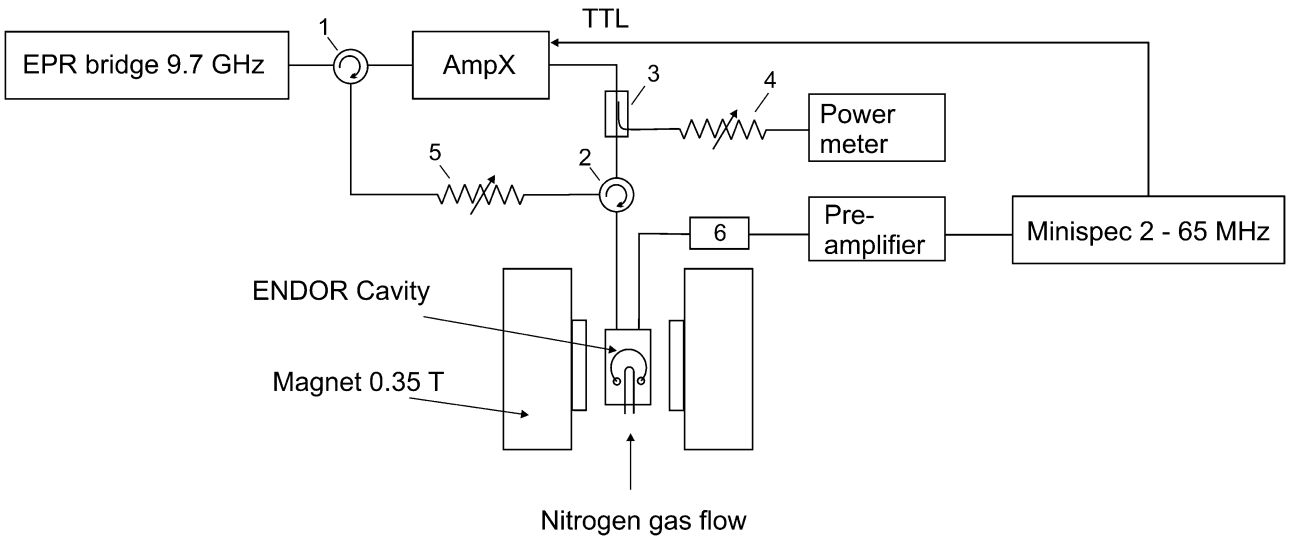

Fig. 1 Low-field DNP setup operating at 0.35 T (9.7 GHz EPR, 15 MHz ^{1}H NMR) consisting of a commercial Bruker EMX X-band EPR spectrometer with an AmpX microwave amplifier and a Bruker Minispec (2–65 MHz). Additional parts are denoted as follows: (1), (2) circulators, (3) directional coupler (20 dB), (4) attenuator (10 dB), (5) attenuator (40 dB), (6) NMR tuning and matching capacitors.

NMR detection system over a wide range of signal intensities, when comparing the enhanced and the Boltzmann signals, the ^{1}H-Boltzmann signals of different sample volumes (2–70 μl) were recorded and compared. The recorded signal intensity depends linearly on the sample volume within the error of the enhancements observed in the DNP experiments.

For DNP at higher magnetic fields (> 3 T) we have assembled a DNP set up at 3.4 T, 94 GHz EPR, 140 MHz ^{1}H NMR. The set up is based on a pulse EPR spectrometer with a 400 mW power upgrade (Bruker ElexSys E680) and an Avance III NMR console (Bruker). Similarly to the 9.7 GHz set up, an ENDOR probe head (Bruker EN600-1021H TeraFlex®) with additional RF tuning and matching devices was utilized. The length of the TE_{011} cylindrical resonator at 94 GHz is around 4–5 mm and its diameter is slightly larger than 4 mm. Such small dimensions combined with the limited penetration depths of the 94 GHz microwave in water (0.24 mm) dictate the sample size of 0.1 mm inner diameter (ID).

4-Oxo-TEMPO-D_{16},1-^{15}N free radical (TEMPONE-D,^{15}N) was dissolved in distilled water at concentrations 5, 10, 25 and 50 mM and the NMR ^{1}H signal of the water molecules was detected. The radical with labelling degree 98% (D, ^{15}N) was purchased from Sigma Aldrich and was used without further purification. The solutions were subsequently flushed with nitrogen for 10 min to remove residual oxygen from the sample. To test the effect of the sample geometry on the magnetic and electric field distributions in the cavity and consequently on the DNP enhancements, three different sample sizes were used. We started with the standard 0.9 mm ID (1.5 mm outer diameter OD) tubes filled up to a height of 10 mm, as used at X-band for aqueous solutions, then reduced the ID to 0.45 mm (1.2 mm OD) with a height of 10 and 3 mm respectively. The size of the smallest sample fitted entirely in the homogeneous B_1 region of the resonator. The exact position of the tiny sample was adjusted by observing and maximizing the intensity of the nitroxide FID while inserting the sample into the resonator at different depths. For all three samples the experimental parameters, such as the effective B_1 and saturation factor on one line, heating effects and DNP enhancements were determined and compared.

Results and discussion

Effective B_1 field and saturation measurements

The first parameter that we determined was the effective B_1 field at the sample position for the three different sample sizes. We recorded FID-detected transient nutations on a 1 mM aqueous solution of trityl radical under identical conditions as in DNP experiments with the TEMPONE radical. The reason for using the trityl radical consisted in its longer relaxation times, which permit the FID detection under critical coupling of the cavity. Representative nutation curves at a microwave power of 5 W are presented in Fig. 2. From the nutation period, the B_1 field was deduced using $\omega_{nut} = \gamma_S \cdot B_1$. The conversion factor c^2Q is given by $B_1^2 = c^2 \cdot Q \cdot P_{mw}$ and was determined from a linear fit of ${B_1}^2$ over P_{mw} for each sample geometry. The values are given in the figure. The B_1 value perceived by the sample depends on its geometry, *e.g.* at 5 W microwave power the B_1 varies from 4 G in the 0.9 mm ID tubes (10 mm sample length) to 4.5 G or 4.8 G in the 0.45 mm ID tubes with 10 or 3 mm sample length, respectively. This effect needs to be considered when comparing the enhancements for different sample geometries.

The effective B_1 field at the sample directly determines the saturation factor achievable in the DNP experiments. Therefore, we first examined the saturation behaviour of the single hyperfine line *via* its characteristic parameters such as the line intensity and line width as a function of the microwave power. We recorded a series of EPR spectra and the peak-to-trough intensity of the EPR line y' was plotted over the square root of the power (Fig. 3, inset). For three different sample concentrations (5, 10 and 25 mM) the data clearly showed the typical behaviour of a line reaching saturation at the highest available power. We fitted the behaviour using the expression derived

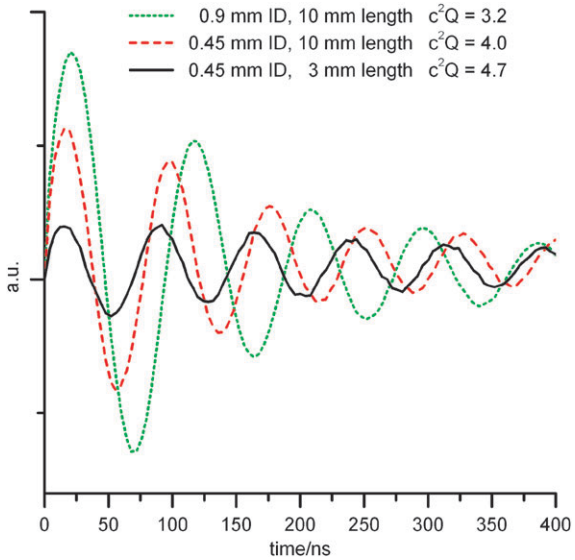

Fig. 2 FID detected transient nutation curves measured with 1 mM trityl under DNP conditions at 5 W microwave power. The corresponding B_1 fields were deduced from the period of oscillation and the conversion factor $c^2 \cdot Q$ was determined from a linear fit of ${B_1}^2$ over P_{mw}.

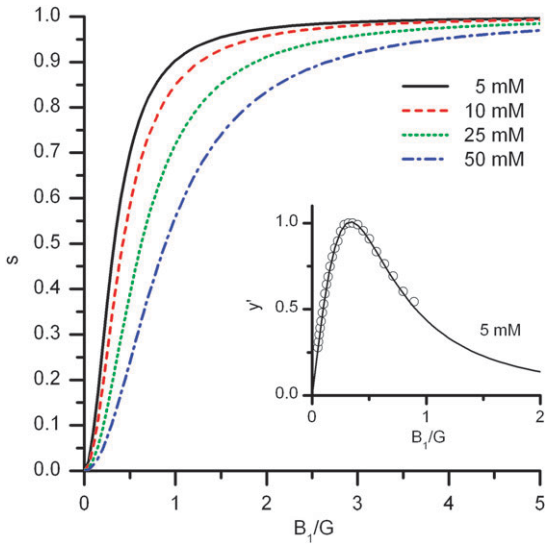

Fig. 3 Saturation factor according to eqn (3) of the pumped hyperfine line at four different concentrations of TEMPONE-D,^{15}N. T_{1e} was measured by a pulsed recovery experiment, T_{2e} was determined from the line width of the cw spectrum. Inset: EPR saturation curve for 5 mM. (○) Measured EPR intensity, (—) Fit according to eqn (2).

from the Bloch equations for the derivative of a Lorentzian line:[23]

$$y' = \frac{y'_0 B_1}{(1 + \gamma_S^2 T_{1e} T_{2e} B_1^2)^{3/2}} \qquad (2)$$

in which γ_S is the gyromagnetic ratio of the electron and T_{1e} and T_{2e} are the longitudinal and transversal electronic relaxation times. y'_0 is the slope of the curve below saturation as deduced from the linear range of the curve. From the fit, the product of the electronic relaxation times $T_{1e} \cdot T_{2e}$ could be obtained. Since T_{2e} was deduced from the linewidth of the cw EPR spectrum (Table 1) T_{1e} resulted in a value of 170 ns.

For comparison, T_{1e} was also measured by an inversion recovery experiment, in which the FID was recorded as a function of the time delay after the inversion pulse. The trace was fitted by a biexponential function in order to account for spin–lattice relaxation and spectral diffusion (not shown). This experiment yielded a larger value for T_{1e} of 350 ns, in agreement with values reported in the literature.[24]

We employed the latter T_{1e} value to explicitly calculate the saturation factor of the irradiated hyperfine line according to:

$$s = 1 - \frac{1}{1 + \gamma_S^2 T_{1e} T_{2e} B_1^2} \qquad (3)$$

and the obtained values are displayed in Fig. 3 as a function of B_1 for the three different radical concentrations. The plot clearly indicates that the saturation factor reaches the maximal value of unity for all four concentrations at the maximal available B_1 field.

Pulse ELDOR experiments

In order to determine the saturation degree of the hyperfine line next to the pumped line, which contributes to the effective saturation factor in eqn (1), we performed a pulse ELDOR experiment with a 5 and 10 mM TEMPONE-D, ^{15}N solution (the FID of a 25 mM solution was not detectable due to the short relaxation times at this concentration). The data are displayed in Fig. 4. A 100 ns pump pulse with a B_1 strength of 2 G was set on the ELDOR frequency and this frequency was swept through the EPR resonance while detecting the intensity of the EPR FID. When the ELDOR pulse was on resonance with the detected line, the FID disappeared as expected under saturation (left line in ELDOR spectrum). When the ELDOR pulse became resonant with the second hyperfine line, the decrease in the FID was 62 ± 3% and 55 ± 3% for the 10 and the 5 mM sample concentrations, respectively (Fig. 4). This let us calculate an effective saturation factor for both lines of 0.81 ± 0.03 and 0.77 ± 0.03. The ELDOR effect might be even larger for a 25 mM solution, as it is expected to be concentration dependent.[25]

To rationalize the observed ELDOR effects, we recalled the theory developed by Freed[25,26] on the saturation behaviour of coupled hyperfine lines. In those papers, it was noted that within two coupled hyperfine lines, the saturation can be transferred from one line to the other *via* spin-relaxation processes. In a four-level system of an electron spin coupled to a nuclear spin $\frac{1}{2}$, for a limiting case in which the nuclear spin lattice relaxation T_{1n} is much faster than the electronic T_{1e}, the saturation of a pumped line can be entirely transferred to the second line. Although this case seemed unrealistic, it was reported later on by Robinson *et al.*[27] that indeed it occurs for nitroxide radicals in a certain temperature range. At room temperature, T_{1n} and T_{1e} for a 0.5 mM solution of ^{15}N-TEMPOL were found to be very similar, *i.e.* up to $T_{1e}/T_{1n} = 0.8$.[27] Generally, for a four-level system, the reduction R [(signal with pump off) − (signal with pump on)/(signal with pump off)] in the intensity of one hyperfine line when saturating the second line was given analytically to:[25]

$$R = 1 - \frac{2}{2 + W} \qquad (4)$$

Table 1 Summary of experimental and calculated data for a 0.45 mm ID sample tube and $B_1 = 4$ G

Concentration/mM	T_{2e}/ns	t_{mw}/s	ε_{obs}	s (one line)	s (both lines)	T_{max} from ΔQ^a/°C	ξ at T_{max} from eqn (1)^b
5	86	4	-148 ± 12	0.99	0.77 ± 0.03	40 ± 3	0.38 ± 0.04
10	52	2	-160 ± 10	0.99	0.81 ± 0.03	36 ± 3	0.34 ± 0.03
25	25	1	-169 ± 9	0.97	—	27 ± 3	≤ 0.34
50	13	0.5	-165 ± 14	0.95	—	24 ± 3	≤ 0.32

[a] The error of T_{max} was estimated from the scatter of the measured and calculated values. [b] f was taken from the accompanying paper (Luchinat *et al.*). For the two concentrations where no effective saturation factors were available, the saturation factor of the 10 mM sample was used as a lower estimate.

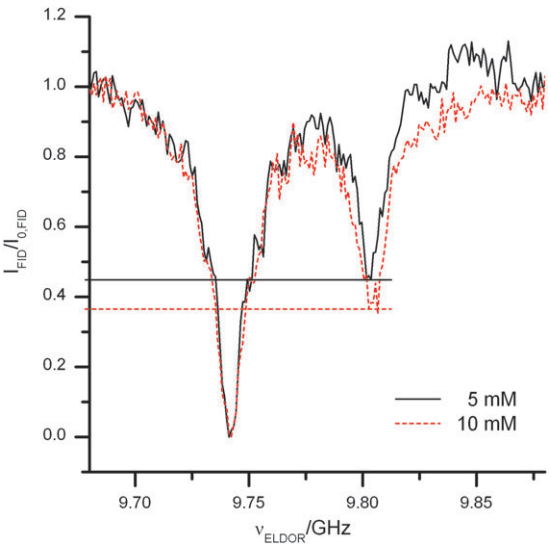

Fig. 4 Normalized FID intensity of TEMPONE-D,^{15}N at the high-field hyperfine line while sweeping the ELDOR frequency ν_{ELDOR} over the EPR spectrum.

with

$$W = \frac{W_n}{W_e} + \frac{W_{exc}}{2 \cdot W_e} \quad (5)$$

where $W_n = 1/T_{1n}$, $W_e = 1/T_{1e}$ and W_{exc} is the rate of Heisenberg and chemical exchange. If we insert the above mentioned ratio for ^{15}N-TEMPOL at RT, our T_{1e} value of 350 ns and W_{exc} per concentration $\approx 2.2 \times 10^9$ M^{-1} s^{-1} from ref. 28 (as also discussed by Sezer *et al.*[29]) we obtain $R \approx 0.6$ and $R \approx 0.7$ for 5 and 10 mM, respectively. This result is well consistent with our ELDOR data within the experimental error.

Dielectric losses and heating effects

Another important issue for the discussion of DNP enhancements is the severe MW heating of aqueous samples which could damage the sample but also hamper the proper evaluation of the coupling factor. In a first attempt to estimate the heating in our samples, we used a Neoptix Nomad™ fiber optical thermometer with a modified Neoptix T1™ optical temperature sensor. It was possible to monitor the sample temperature during microwave irradiation, however only in larger capillaries with 0.9 mm ID (6 µl sample volume). Fig. 5 shows the maximum temperature that was reached during microwave irradiation starting from room temperature with and without N_2 gas flow. The two curves are essentially identical. This indicates that the nitrogen flow does not cool the sample itself but can only dissipate the heat from the cavity to keep the resonance conditions stable. We observe that the heating of the sample strongly depends on the duration of irradiation and amounts to $\sim$10 K when irradiating for 0.5 s in the large sample tubes (0.9 mm ID).

An alternative way to quantify the heating of the sample consists in calculating the energy absorbed by the sample *via* the change in the cavity quality factor. This method has the advantage that it can also be applied to the small sample tubes and can be compared to the direct temperature measurement with the larger tubes. The change of the sample temperature is given by $\Delta T = \Delta E/C$, where ΔE is the absorbed energy and C the heat capacity of the sample.

The change of the quality factor can be determined by evaluating the full width at half maximum (FWHM) of the cavity dip $\Delta\nu$ with respect to the FWHM of the empty cavity $\Delta\nu_0$ and gives a measure of the fraction of energy that is stored in the sample.[23] Hence,

$$\Delta E = \frac{\Delta\nu - \Delta\nu_0}{\Delta\nu_0} P_{mw} t_{mw}. \quad (6)$$

The energy is distributed among the aqueous sample itself and the glass surrounding the sample. If we assume that the

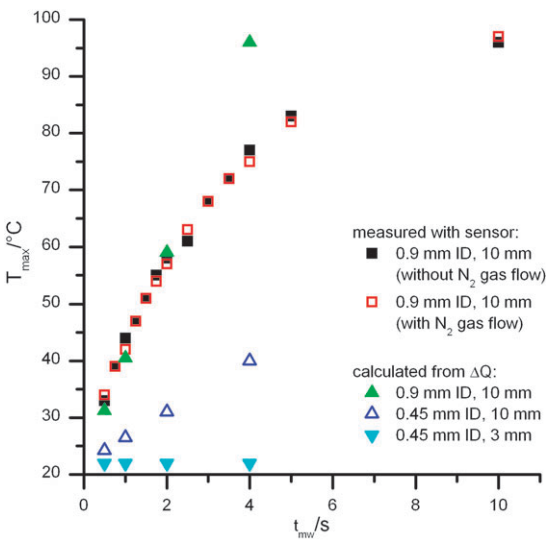

Fig. 5 Temperature of the sample during different microwave irradiation times t_{mw} for $P_{mw} = 4$ W and different tubes and filling heights of aqueous solution at X-band. The data were either directly measured by a temperature sensor (■) or calculated from the observed shift in the cavity Q factor (▲).

temperature of the two is equilibrated the heating of the sample is given by

$$\Delta T_{\text{sample}} = \frac{\Delta E}{C_{\text{water}} + C_{\text{glass}}}. \quad (7)$$

The dip of the microwave cavity was monitored for the empty resonator and when samples of different geometries were inserted. The dip was recorded several times for each sample geometry and the heating was calculated for the power (P_{mw} = 4 W) and for the irradiation times used in the DNP experiments of t_{mw} = 0.5–4 s. The sample temperature calculated with $C_{\text{water}} = c_{\text{water}} \cdot n_{\text{water}}$ and $C_{\text{glass}} = c_{\text{glass}} \cdot m_{\text{glass}}$ is displayed in Fig. 5. Here c_{water} = 75.3 J/(mol K) and c_{glass} = 0.7 kJ kg^{-1} K^{-1}) are the specific heat capacities, whereas n_{water} and m_{glass} are the number of moles of the water molecules and the mass of the part of the tube surrounding the sample volume, respectively. The ΔT values for a 0.9 mm ID tube filled to a height of 10 mm with aqueous sample range from 15 to 25 °C at t_{mw} = 1 s and are in excellent agreement with the value directly measured with the temperature sensor. For the 0.45 mm ID tubes filled to a height of 10 mm the heating ranges from 0 to 8 °C for 1 s of microwave irradiation. No change in the Q factor and consequently no heating was observed for the 0.45 mm ID tubes filled to a height of 3 mm. This means that microwave heating can be kept at minimum when utilizing sample tubes of 0.45 mm ID.

DNP experiments

In the DNP experiments, the proton NMR signal preceded by microwave irradiation was compared to the Boltzmann signal measured without microwave irradiation. Due to the small sample volume, the Boltzmann signal was recorded averaging many FIDs (usually 1024 scans for a 10 mm sample in a 0.45 mm ID tube) whereas the DNP enhanced signal was clearly visible in a single scan. For the latter, we used an average of 8 scans to complete a full phase cycle.

For careful measurement of NMR signal intensities two methods have been used in the literature: either the evaluation of the first point of the FID or the integral of its Fourier transformation. Both methods are in principle equivalent, however we noted at X-band that the oscillation frequency of the FID changes during the long accumulation of the Boltzmann signal because of magnetic field instabilities. Subsequently, the sum of the accumulated FIDs undergoes a shorter decay time giving rise to broadening of the Boltzmann signal as compared to the DNP signal. The use of an FF lock connected to the EPR spectrometer considerably alleviates the issue but does not suppress it entirely. Therefore, we found that the comparison of the first points of the respective FIDs provides the most accurate results. A typical DNP measurement is displayed in Fig. 6 and reports a DNP enhancement of −170 directly observable from the ratio of the FID intensities.

The DNP enhancements were recorded as a function of the sample concentration, the microwave power (*i.e.* the B_1 field) and the sample size. In a first diagram (Fig. 7a) we illustrate the effect of the sample heating and the magnetic field instabilities for one representative sample concentration of 30 mM and two sample sizes, 0.9 and 0.5 mm ID tubes with

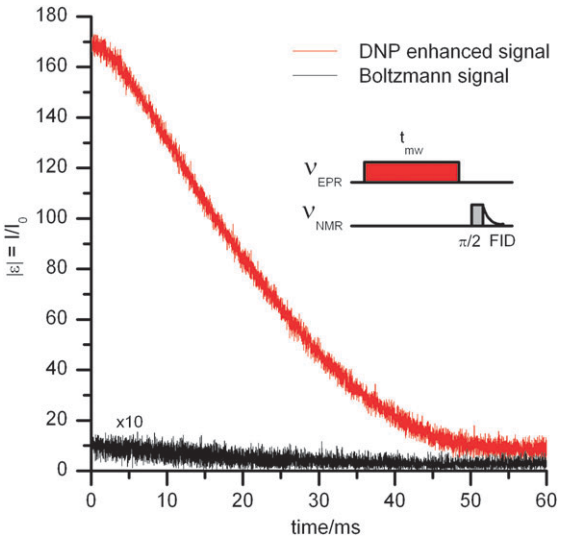

Fig. 6 Magnitude of the NMR FID with and without microwave irradiation. Comparison of the first points of the respective FIDs results in an enhancement of ε = −170. A 25 mM radical concentration was utilized with t_{mw} = 1 s. The sample was filled up to 3 mm height into a 0.45 mm ID sample tube. The Boltzmann signal required 4096 scans whereas the DNP enhanced signal was recorded within 8 scans.

10 mm filling height. No FF lock and cooling gas were used. We observe that the enhancements increase with power until reaching a steady state value of around −170. First, if we compare these data with the ones published by Höfer *et al.*[14] under identical conditions (for 0.9 ID tubes) we find that they are entirely reproducible. In those measurements, a maximum power of 4 W was used and a maximal enhancement of −140 was reported. It was stated that the enhancement was power limited, which is indeed demonstrated in the present experiment.

Secondly, at intermediate power the enhancements in the 0.9 ID tube exceed the ones for the 0.5 mm ID tube by about 10%. The difference can be assigned to heating effects, which increase the coupling factor. Our experiments depicted in Fig. 5 indicate that the temperature in the 0.9 mm tube is about 10 °C higher than in the 0.45 tube for an irradiation of 750 ms. Independent NMRD experiments (see accompanying paper, Luchinat *et al.*) indicated that the coupling factor rises by about 10% between 298 and 310 K, which is totally consistent with the present DNP data.

Fig. 7b illustrates the concentration dependence of the enhancements as a function of power for the smaller sample tubes (0.45 mm ID, 10 mm length). In addition, nitrogen cooling and an FF lock were employed. Overall, the enhancements are now shifted to lower power and the steady state value of −170 is reached at about 4 W at high concentrations (25 mM, 50 mM). The effect is assigned to a more precise irradiation on the maximum of the EPR line provided by the FF lock and the cooling of the cavity. As expected from the saturation behaviour of one line in Fig. 3 the lower concentrated samples are faster saturated and therefore reach saturation at lower power. However, due to less saturation transfer to the second line (see Fig. 4), they attain a lower

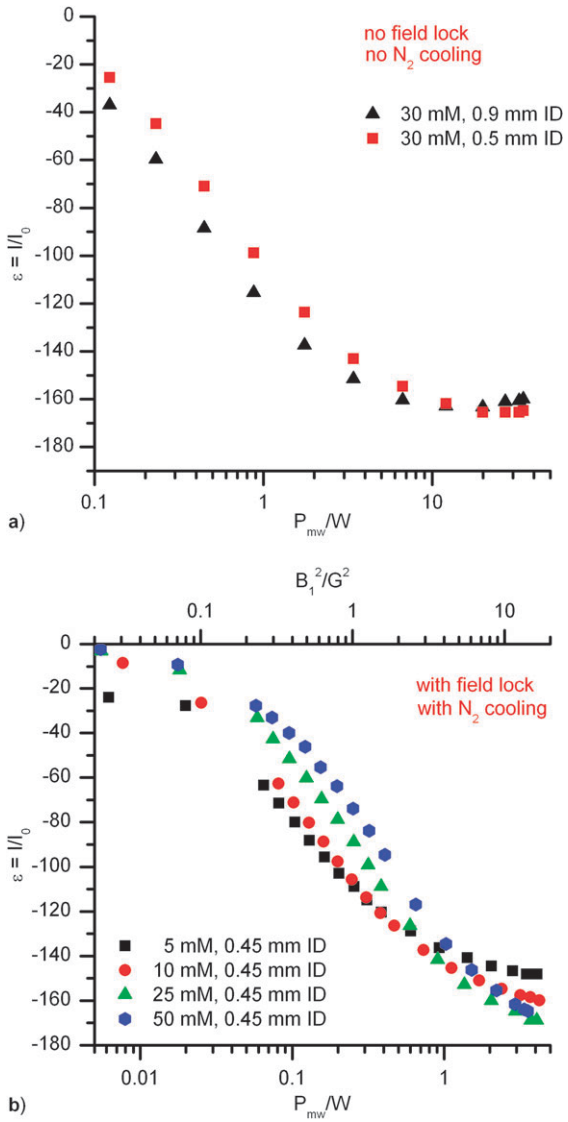

Fig. 7 (a) Power dependence of the enhancement factor with the 40 W microwave amplifier. Experimental conditions: t_{mw} = 750 ms, number of averages: 16 (DNP signal), 10 000 or 20 000 (Boltzmann signal) for 0.9 mm ID or 0.5 mm ID tubes, respectively. (b) Power dependence of the enhancement for several polarizer concentrations. t_{mw} ranges from 0.5 to 4 s depending on the radical concentration. Experimental conditions: number of averages: 8 (DNP signal), 1024 (Boltzmann signal).

maximum enhancement than the higher concentrated samples (see also Table 1). Finally we observed that also the smallest sample (0.45 mm ID and 3 mm height) shows a maximum enhancement of −170, for which no temperature effect could be detected.

The observation of a steady state enhancement for all concentrations at very high power gives evidence that the enhancement is saturated under our experimental conditions. This indicates that a limit for the effective saturation factor is reached, as the pumping line is saturated.

Our data permit now to rationalize the observed enhancements in a quantitative way according to the Overhauser eqn (1). The enhancements and the effective DNP saturation factors can be used to calculate the coupling factors at the corresponding experimental temperature. The leakage factors for each concentration and temperature are obtained from NMR data (Luchinat *et al.*, this issue). The results are summarized in Table 1. We find compelling agreement between our calculated values and the NMRD ξ ones (*i.e.* ξ_{NMRD} = 0.36 for 5 and 10 mM concentration and ξ_{NMRD} = 0.33 for 25 and 50 mM, taking into account the observed temperature rise in Table 1). However, we point out that we still cannot distinguish between the small differences predicted by the MD calculations of ref. 22 as compared to the NMRD (for instance, ξ_{NMRD} = 0.33 *versus* ξ_{MD} = 0.30 at room temperature). Finally, our results unambiguously discard the previously proposed coupling factor of 0.22 in ref. 21 and support our working protocol that the experimental parameters in eqn (1) are best determined in an independent fashion.

W-band DNP

DNP experiments at W-band were performed to test whether we would observe larger enhancements as we previously reported (ε = −20) if using a power upgrade module (400 mW) and the ^{15}N-labelled radical, which can be better saturated than the ^{14}N-based one. Samples were irradiated by a microwave pulse for 1 s on the low field line (Fig. 8b) and the subsequent NMR FID was recorded. The experiments were performed without active cooling, due to the restricted access of the gas flow into the cavity.

Fig. 8a shows the Boltzmann and DNP enhanced ^{1}H NMR spectra of water containing 25 mM of the radical. The ^{1}H-Boltzmann signal was accumulated for 1024 scans, the DNP signal only 16 scans. To quantify the DNP effect it was necessary to subtract the background signal of the empty cavity, which was dominant in the ^{1}H-Boltzmann spectra. This could be performed only after Fourier transformation, thus the DNP enhancement had to be evaluated from the intensity of the FT spectra. The line width of the Boltzmann and DNP signal turned out to be almost identical (within 10–15%), so that field drifts are negligible and the signals can be safely compared. The highest DNP enhancement amounted to ε = −43.

As we pointed out in the previous section, it is important to relate this enhancement to a specific sample temperature. The small sample size does not allow an access to a temperature sensor and further the resolution of the NMR detection at 3.4 T is not sufficient to monitor the NMR line shift of the water protons. Therefore we estimated the temperature by measuring the reduction of the cavity quality factor. The Q factor of the empty W-band resonator was measured to be 5800, whereas the value with the sample tube inserted was 5200. According to eqn (6) and (7), the shift yields an increase in temperature of about 15 K. However, we note that the error might be large due to the very small volume of the sample.

In order to fully define the conditions for which the enhancement is reported, we measured the B_1 field at the sample with transient nutation experiments on a 5 mM TEMPONE-D, ^{15}N, (Fig. 8c). The B_1 produced with the 400 mW microwave power upgrade amounted to 4.9 G and is comparable to the one achieved at X-band. For the same sample, the T_{1e} value

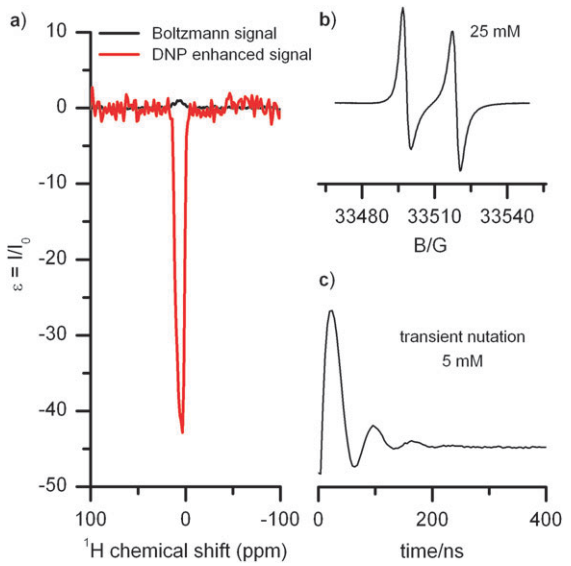

Fig. 8 (a) ^{1}H NMR spectra of water containing 25 mM TEMPONE-D,^{15}N at W-band. Exp. conditions: B_1 = 4.9 G, 16 scans for the DNP enhanced and 1024 scans for the Boltzmann signal. The spectra were scaled according to the respective number of scans. (b) EPR spectrum of the investigated sample. (c) Transient nutation experiment for determination of the microwave B_1.

was determined in an inversion recovery experiment and resulted in $T_{1e} \approx 350$ ns. This value lies in the range of T_{1e} measured at this frequency with different methods[24,30] and the spread is likely due to the different oxygen content. With the measured B_1, T_{1e} and the T_{2e} values from the EPR line width (low field line), we extract the saturation factor of the irradiated hyperfine line from eqn (3). For a concentration of 25 mM, T_{2e} was 20 ns and $s \approx 0.98$. This value indicates that also at this frequency we have reached saturation of the irradiated line. Although a power dependence of the DNP enhancement could not be recorded with the available hardware, the latter result suggests the DNP enhancement should be close to saturation as well. An examination of the Overhauser eqn (1) together with the reported enhancement of –43 and the leakage and coupling factors from NMRD data at 308–318 K (f = 0.91 and ξ = 0.11, respectively, see accompanying paper, Luchinat *et al.*) let us estimate an effective saturation factor for the whole EPR spectrum of only $s \approx 0.65$. Pulse ELDOR experiments at this frequency are currently underway to support this analysis.

Conclusions

We have described a detailed characterization of a 9 GHz/0.35 T DNP set up for aqueous samples. The work has led to the observation of an enhancement of −170 of water protons at room temperature, the highest ever reported with radicals in solution. We have rationalized this enhancement in terms of the Overhauser equation and the results agree with the predictions from the available theory for EPR saturation. We have concluded that the reported enhancement is expected to be the maximal enhancement achievable for this system with CW irradiation, as saturation of the DNP effect was visible at all radical concentrations used. For comparison, we performed similar experiments at the 10 fold field and frequency, *i.e.* at 3.4 T/94 GHz, and using a comparable B_1 microwave pumping field. The more challenging experimental set up at 94 GHz EPR did not allow to perform all detailed investigations as at X-band, however our data predict that also at this frequency the observed enhancement of −43 is close to saturation. Thus, the maximum achievable enhancement at X-band is only about four times larger than at W-band although a factor of ten in ratio between the frequencies. For future applications of DNP in solution the higher polarizing field, *i.e.* 3.4 T seems more appealing than the lower one, as higher detection fields are required in standard solution NMR and the effective enhancement has to be scaled by the ratio between polarizing and detecting field. For instance, in our proposed shuttle DNP set up[9,10] with ^{1}H detection at 600 MHz, the maximum enhancement achieved at X-band (−170) is scaled by a factor of 40 and we expect maximum effective enhancements of only about −4 at the detecting field. Within the same shuttle concept, a polarizing field of 3.4 T would lead to enhancements of $-43(3.4\ \text{T}/14\ \text{T}) \approx -10$, which is substantially higher. Nevertheless, the lower penetration depth and the higher dielectric losses at this frequency, requiring tiny sample volumes, and the complexity of microwave resonators in the mm wave range aggravate the implementation of such a polarizer set up in a shuttle spectrometer. Progress in microwave technology might render this technique accessible in the future.

Acknowledgements

We would like to acknowledge Thorsten Marquardsen for technical support with the W-band DNP setup. The work has been supported by the EU Design Study Bio-DNP.

References

1 D. Hausser and D. Stehlik, *Advances in Magnetic Resonance*, 1968, **3**, 79–139.
2 W. Müller-Warmuth and K. Meise-Gresch, *Advances in Magnetic Resonance*, 1983, **11**, 1–45.
3 V. S. Bajaj, M. L. Mak-Jurkauskas, M. Belenky, J. Herzfeld and R. G. Griffin, *Proc. Natl. Acad. Sci. U. S. A.*, 2009, **106**, 9244–9249.
4 T. Maly, G. T. Debelouchina, V. S. Bajaj, K. N. Hu, C. G. Joo, M. L. Mak-Jurkauskas, J. R. Sirigiri, P. C. A. van der Wel, J. Herzfeld, R. J. Temkin and R. G. Griffin, *J. Chem. Phys.*, 2008, **128**, 052211–05221119.
5 J. H. Ardenkjaer-Larsen, B. Fridlund, A. Gram, G. Hansson, L. Hansson, M. H. Lerche, R. Servin, M. Thaning and K. Golman, *Proc. Natl. Acad. Sci. U. S. A.*, 2003, **100**, 10158–10163.
6 C. G. Joo, K. N. Hu, J. A. Bryant and R. G. Griffin, *J. Am. Chem. Soc.*, 2006, **128**, 9428–9432.
7 M. J. Prandolini, V. P. Denysenkov, M. Gafurov, B. Endeward and T. F. Prisner, *J. Am. Chem. Soc.*, 2009, **131**, 6090–6092.
8 M. J. Prandolini, V. P. Denysenkov, M. Gafurov, S. Lyubenova, B. Endeward, M. Bennati and T. F. Prisner, *Appl. Magn. Reson.*, 2008, **34**, 399–407.
9 M. Reese, D. Lennartz, T. Marquardsen, P. Höfer, A. Tavernier, P. Carl, T. Schippmann, M. Bennati, T. Carlomagno, F. Engelke and C. Griesinger, *Appl. Magn. Reson.*, 2008, **34**, 301–311.
10 M. Reese, M.-T. Türke, I. Tkach, G. Parigi, C. Luchinat, T. Marquardsen, A. Tavernier, P. Höfer, F. Engelke, C. Griesinger and M. Bennati, *J. Am. Chem. Soc.*, 2009, **131**, 15086–15087.

11 R. D. Bates and W. S. Drozdoski, *J. Chem. Phys*., 1999, **67**, 4038–4044.
12 D. Grucker, T. Guiberteau, B. Eclancher, J. Chambron, R. Chiarelli, A. Rassat, G. Subra and B. Gallez, *J. Magn. Reson., Ser. B*, 1995, **106**, 101–109.
13 P. Höfer, G. Parigi, C. Luchinat, P. Carl, G. Guthausen, M. Reese, T. Carlomagno, C. Griesinger and M. Bennati, *J. Am. Chem. Soc*., 2008, **130**, 3254–3255.
14 P. Höfer, P. Carl, G. Guthausen, T. Prisner, M. Reese, T. Carlomagno, C. Griesinger and M. Bennati, *Appl. Magn. Reson*., 2008, **34**, 393–398.
15 S. Garcia, J. H. Walton, B. D. Armstrong, S. Han and M. J. McCarthy, *J. Magn. Reson*., 2010, **203**, 138–143.
16 A. W. Overhauser, *Phys. Rev*., 1953, **92**, 411–415.
17 A. W. Overhauser, *Phys. Rev*., 1953, **89**, 689–700.
18 C. Luchinat and G. Parigi, *Appl. Magn. Reson*., 2008, **34**, 379–392.
19 B. D. Armstrong and S. Han, *J. Chem. Phys*., 2007, **127**, 104508.
20 B. D. Armstrong, P. Soto, J. E. Shea and S. Han, *J. Magn. Reson*., 2009, **200**, 137–141.
21 B. D. Armstrong and S. G. Han, *J. Am. Chem. Soc*., 2009, **131**, 4641–4647.
22 D. Sezer, M. J. Prandolini and T. F. Prisner, *Phys. Chem. Chem. Phys*., 2009, **11**, 6626–6637.
23 C. P. Poole, *Electron Spin Resonance*, John Wiley & Sons, New York, 1983.
24 J. S. Hyde, J.-J. Yin, W. K. Subczynski, T. G. Camenisch, J. J. Ratke and W. Froncisz, *J. Phys. Chem. B*, 2004, **108**, 9524–9529; W. Froncisz, T. G. Camenisch, J. J. Ratke, J. R. Anderson, W. K. Subczynski, R. A. Strangeway, J. W. Sidabras and J. S. Hyde, *J. Magn. Reson*., 2008, **193**, 297–304.
25 J. S. Hyde, J. C. W. Chen and J. H. Freed, *J. Chem. Phys*., 1968, **48**, 4211–4226.
26 J. H. Freed, *J. Phys. Chem*., 1967, **71**, 38.
27 B. H. Robinson, D. A. Haas and C. Mailer, *Science*, 1994, **263**, 490–493.
28 I. V. Koptyug, S. H. Bossmann and N. J. Turro, *J. Am. Chem. Soc*., 1996, **118**, 1435–1445.
29 D. Sezer, M. Gafurov, M. J. Prandolini, V. P. Denysenkov and T. F. Prisner, *Phys. Chem. Chem. Phys*., 2009, **11**, 6638–6653.
30 W. Hofbauer, K. A. Earle, C. R. Dunnam, J. K. Moscicki and J. H. Freed, *Rev. Sci. Instrum*., 2004, **75**, 1194–1208.